Tidal energy resource assessment in the Strait of Magellan in Chilean Patagonia

Suarez L., Escauriaza C., Guerra, M., Williams, M. E.

Abstract—**Tidal energy industry is reaching maturity, with various pilot sites demonstrating the ability of hydrokinetic devices to generate electricity. As tidal turbines become more reliable, it is important to obtain detailed characterizations of tidal resources at potential sites. The Strait of Magellan, in the Patagonia region of Southern Chile, is an inland connection between the Pacific and the Atlantic Oceans with strong tidal currents. To assess the magnitude of the tidal energy resources in this area, field surveys including Acoustic Doppler Current Profilers (ADCP), and tidal gauge measurements were carried out in the vicinity of a narrows in the strait. The data helped to validate a detailed numerical model to assess the hydrodynamic characterization of the area.**

Keywords— **field survey, numerical modelling, tidal resource assessment, tidal energy potential.**

I. Introduction

The Strait of Magellan in Chilean Patagonia (Lat: 53.5°S) connects the Atlantic with the Pacific Oceans through a narrow passage. Stress from navigation, oil and coal industries combined with changes due to anthropogenic climate change and local population growth make the region both complex and relevant to the marine energy industry. A large difference in tidal range between the Atlantic and the Pacific ends of the strait gives rise to strong currents that have a significant potential for hydrokinetic energy. Maximum currents up to 4.5 m/s have been observed in two of the Strait constrictions, known as the First and Second narrow (Fig. 1) [1]. However, the dynamics of this system controlled by the strong tidal forcing influenced mainly by the tidal range on the Atlantic side still remains unexplored.

Although there exists some numerical modelling around the area, mainly focused on the Patagonian shelf [2,3] and the Magellan plume [4], there exist some numerical modelling that includes the strait of Magellan but at a large scale [5,6]. The first study on numerical modelling of the strait of Magellan with the Princeton Ocean Model with a curvilinear grid and sigma coordinates for the vertical [7] shows a net transport towards the Atlantic side and the influence of wind for the local transport.

The main goal of this investigation is to perform a detailed assessment of the tidal energy potential of the Strait. Field measurements are combined with FVCOM (Finite Volume Community Ocean Model [8]) numerical simulations to assess the tidal energy potential and to understand the complex physical aspects of the system. This model has been used and validated for the estimation of tidal current energy resources [9,10,11,12]. To our knowledge, this is the first numerical modelling focused on marine energy for the Strait of Magellan.

Two field experiments were conducted during 2018 and 2019 to characterize the flow of the Strait's Second narrows (Figs. 1 and 2). The collected field data is critical to understand the factors that control the dynamics of the flow in this section of the channel, and to understand its marine energy potential. Measured velocities are used to calibrate and validate a FVCOM numerical model, which will expand the spatial and temporal knowledge obtained by the measurements and will allow for the estimation of tidal energy resources for the entire Strait of Magellan, and to evaluate the impacts of varying climate conditions in the area.

II. Material and Methods

A. Study site

The Magellan strait is a tidal channel that connects the Atlantic Ocean and the Pacific Ocean located in the Chilean Patagonia (Fig. 1 and Fig. 2). On the Atlantic end of the channel, the tidal amplification results in tidal

L. Suarez is with the Marine Ernegy Research and Innovation Center (MERIC), Av. Jose Escriva de Balaguer 13.105, Of. 1011, Lo Barnechea, Santiago, Chile (e-mail: leandro.suarez@meric.cl).

C. Escauriaza is with the Hydraulic and Environmental Engineering Department, Pontificia Universidad Católica de Chile, Av. Vicuña Mackenna 4860, Santiago, Chile. (e-mail: cescauri@ing.puc.cl)

M. Guerra is with the Department of Civil Engineering at Universidad de Concepción and with Center for Oceanographic Research COPAS COASTAL, Barrio Universitario s/n, Concepcion, Chile (e- mail: marguerra@udec.cl).

M.E. Williams is with the Biological Sciences Faculty, Pontificia Universidad Católica de Chile, Avda. Libertador Bernardo O'Higgins 340, Santiago, Chile. (e-mail: mwilliams@bio.puc.cl)

Digital Object Identifier: https://doi.org/10.36688/ewtec-2023-570

ranges between 7 and 9 m, while on the Pacific end of the channel, the tidal range is about 1 m. This difference in tidal ranges generates strong currents in the two narrows shown in Fig. 1, peaking at 4.5 m/s [1]. Previous studies have shown that the net flux of water through the Strait of Magellan is towards the Atlantic [13].

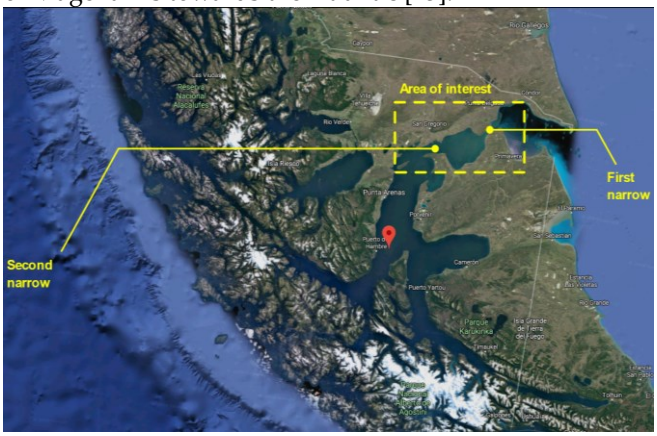

Fig. 1. Area of interest of the Strait of Magellan, which connects the Pacific Ocean on the west and the Atlantic Ocean on the east. There are two narrows in the Magellan strait with high velocities potentially suitable for marine energy.

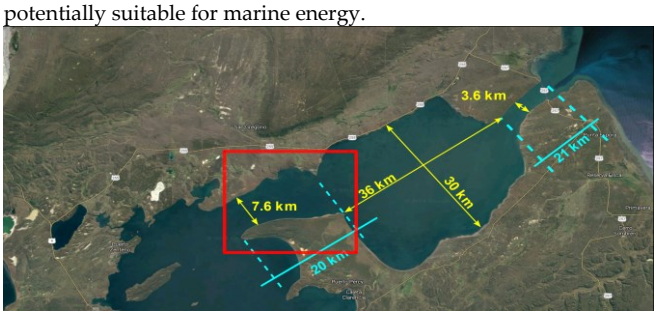

Fig. 2. Dimensions of the eastern section of the Strait of Magellan, including the two narrows. The red rectangle shows the area of the field survey, shown in detail in Figure 3.

B. *Field measurements*

A field survey was conducted in the Second narrows (red rectangle in Fig. 2) during March and April 2019. The detailed locations of the field measurements are shown in Fig 3.

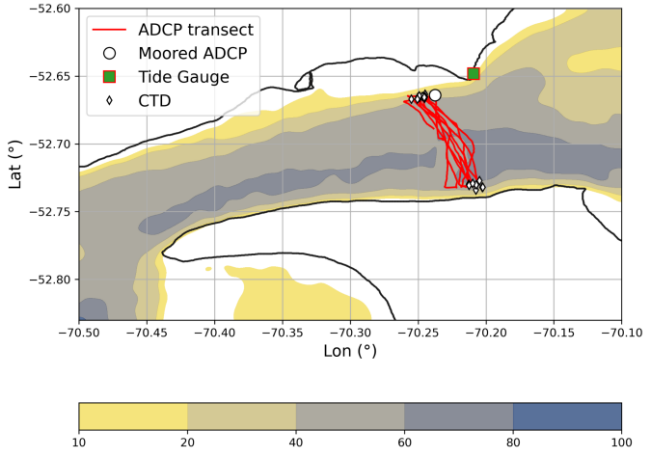

Fig. 3. Overview of the measurements made in the Strait of Magellan" Second narrow. The contour lines represent the isobaths in meters, the red lines the vessel-mounted ADCP transects. The bottom-mounted ADCP location is indicated by the white circle and the San Gregorio tidal gauge is denoted by a green square. The white diamonds represent the position of the CTD (Conductivity Temperature Depth) measurements conducted during the ADCP transects.

A range of flow parameters were measured during the field experiment. A bottom-mounted ADCP was used to measure turbulence and mean flow velocities. A vessel-mounted ADCP was employed to measure velocities along multiple transects covering the second narrow width. In addition, CTD profiles together with micro-structure turbulence using a Vertical Microstructure Profiler (VMP) were also collected at the end of each transect, but their analysis will be reported in a future communication. In this paper we focus on the ADCP measurements, and the data integrated with the FVCOM numerical simulations.

A Nortek Signature 500 kHz ADCP was deployed at the bottom of the channel (52.664°S, 70.238°W), at a mean depth of 47 m. The ADCP measured both average and burst velocities between March 5, 2019, and April 13, 2019. The ADCP sampled horizontal velocities at 1 Hz for 87 seconds every 30 minutes, using 30, 1.8 m depth cells and a blanking distance of 0.5 m. The burst measurements aimed at measuring the local turbulence dynamics. The ADCP measured along-beam velocities at 2 Hz for 1024 s every 90 minutes using 54, 1m depth cells and a blanking distance of 0.5 m. This combined approach was used to measure both turbulence and mean-flow velocities for an extended period of time.

The vessel-mounted (downlooking) ADCP, a Teledyne RDI Workhorse Sentinel 600 kHz, sampled a vertical profile of horizontal velocity every 5 seconds using 59, 1 m depth cells. The bottom track was used to get the true water velocities. GPS data from the vessel was recorded and integrated to get the location of each velocity profile. Two cross-channel transect surveys were conducted between March 10 and March 13 2019. The first survey occurred on March 10 and lasted 8 hours. The second survey occurred on March 12 and lasted 13 hours. The transect tracks are shown in Fig. 3. The transects began around the position of the bottom-mounted ADCP (north narrow boundary) and extended to the narrow southern boundary. The transects occurred between longitudes -70.25 and -70.20.

C. *Numerical model*

To estimate the tidal energy resource available within the Strait of Magellan, a numerical model based on FVCOM was developed, which has been widely used for modeling coastal systems with complex bathymetry. The model provides an accurate spatial and temporal prediction of currents (and tidal energy potential) within the Strait of Magellan, allowing for the detection of energetic sites, which are potentially suitable for tidal energy extraction.

The developed unstructured numerical grid is shown in Fig. 4. It covers the entire Strait of Magellan, including

its small channels and bays. It is bounded by the Pacific Ocean on the west and by the Atlantic Ocean on the east. The reason to cover such a wide area is for the boundary to reach the open ocean, so that the tidal forcing can be obtained by harmonic analysis with fewer non-linearities. The numerical model is made of about 18.000 nodes and 31.000 cells, and the resolution of the grid ranges from 5000 m in the boundaries to 100 m in the narrowest regions of the strait. A zoom view of the grid at the study area is shown in Fig. 5.

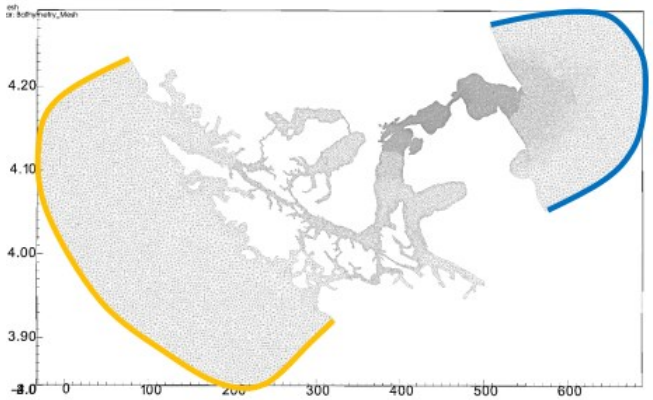

Fig 4. Extent of the numerical model grid. The Pacific boundary is marked by the orange line, the Atlantic boundary is marked by a blue line.

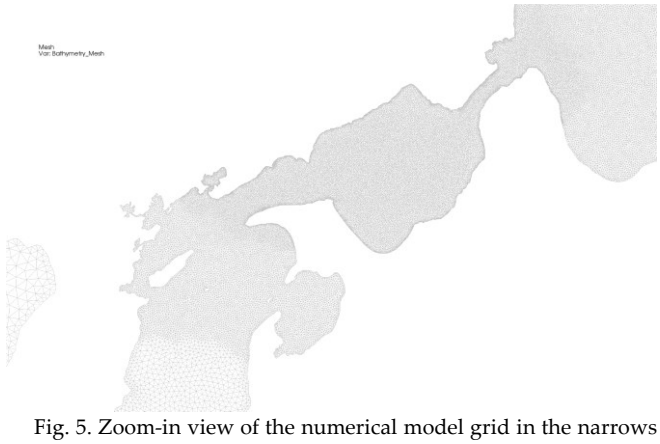

Fig. 5. Zoom-in view of the numerical model grid in the narrows region of the strait, with a grid resolution of up to 100 m.

The bathymetry for the numerical model is constructed using data from GEBCO [14] and from the nautical charts of the Hydrographic and Oceanographic Service of the Chilean Navy (SHOA). The available bathymetry at the study area is shown in Fig. 6.

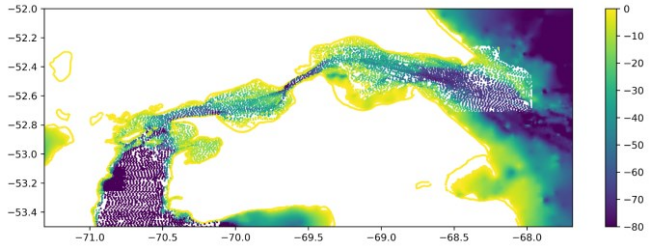

Fig. 6. Bathymetry data (m) available for the study area in the Magellan strait.

The model is solely forced by tides. Tidal astronomic forcing is estimated using the TPXO 7.2 model [15]. The tidal variations used to force the model are presented in Fig. 7. The tidal range at the Pacific boundary is about 1 m, while the tidal range in the Atlantic side is about 8 m, this difference in tidal range is the main driver of the strong currents of the Magellan strait. The model was run for two months coinciding with the deployment of the bottom-mounted ADCP. The data obtained from the model was processed using PyFVCOM toolbox [16].

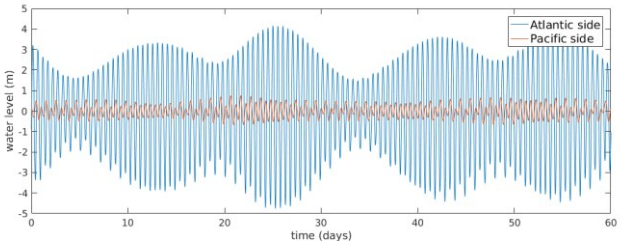

Fig. 7. Tidal astronomical forcing for the Pacific Ocean boundary in orange and the Atlantic Ocean boundary.

III. RESULTS

A. *Field Measurements*

The free-surface elevation (obtained from the bottom-mounted ADCP pressure record) and the measured depth averaged velocities for the 38-day deployment are shown in Fig. 8. In these plots eastward velocities are positive and westward velocities are negative. During spring tides, the tidal range is about 4 m, and during neap tide the tidal range is around 2 m. A strong flow asymmetry is observed in the measurements. The flow is stronger westward, with depth averaged velocities up to 2.4 m/s while maximum velocity is 1.6 m/s eastward during spring tides. During neap tides, the flow asymmetry magnitude is reduced, with similar westward and eastward velocities of about 1 m/s.

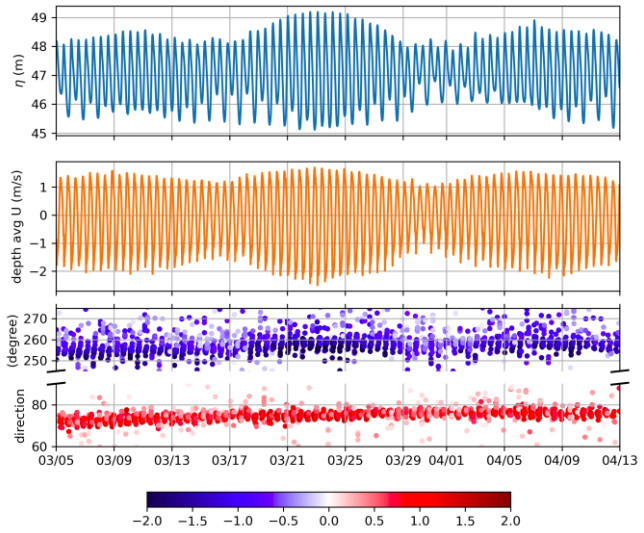

Fig. 8. Tidal elevation, depth averaged velocity magnitude and flow direction from the bottom-mounted ADCP measurements. Negative velocities are westward.

Fig. 9 shows a portion of the bottom-mounted ADCP data during the vessel-mounted ADCP transects. During this period, the tidal range was about 3 m, with eastward

and westward depth averaged velocities reaching 1.4 m/s and 2 m/s respectively. As seen in these plots, the tide behaves like a standing wave, where tidal elevation and tidal currents are approximately in phase. Here, high tide corresponds with westward currents and low tide corresponds with eastward currents.

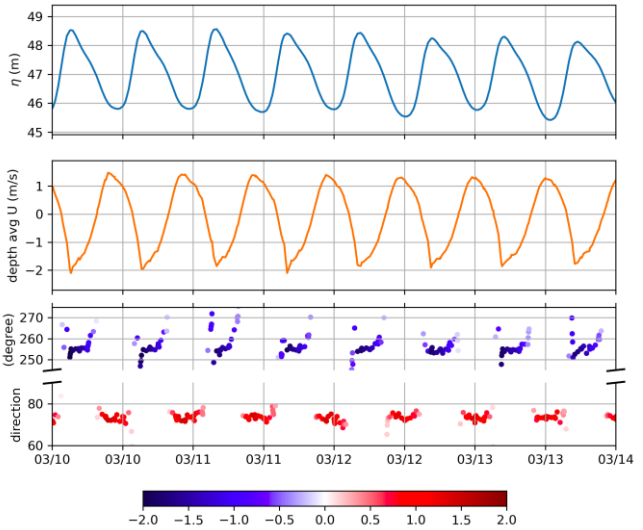

Fig. 9. Tidal height and depth averaged velocity magnitude from moored ADCP during the period of the ADCP transects. Negative velocities are oriented westward. Tidal height and depth averaged velocity magnitude from moored ADCP

Fig. 10 shows velocity measurements collected at different depths by the bottom-mounted ADCP. We observe higher velocities and higher spread (variability in the velocities) to the west, whereas to the east the velocities are in the same direction with a smaller spread.

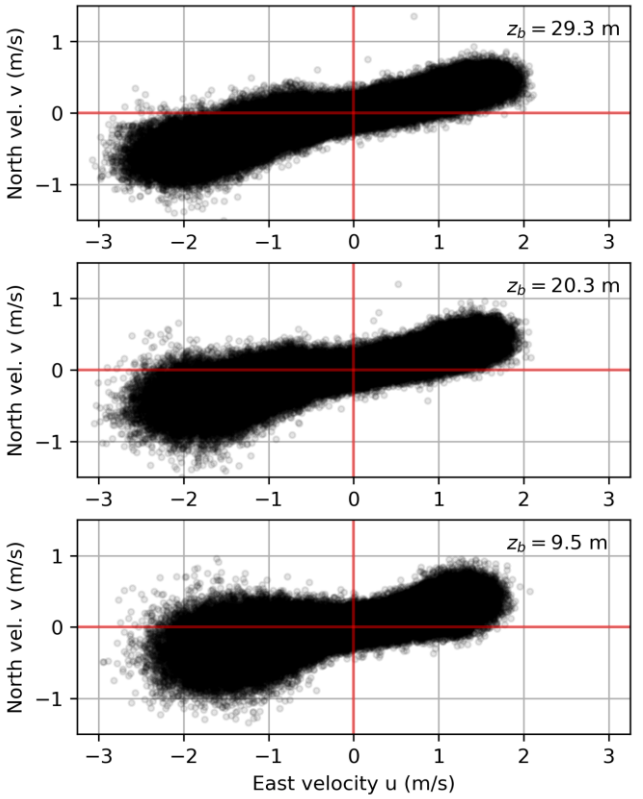

Fig. 10. Instantaneous velocity measurements from the bottom-mounted ADCP at three different depths over the entire measurement period. u and v are the east and north (true) velocity components respectively.

The ship transects, as well as their location tracks and the bottom track depth are shown in Fig. 11. The cross-section bathymetry is about 60 m deep, with steep slopes near the boundaries. The top panel of Fig. 11 shows the depth-averaged current magnitude and direction during each transect.

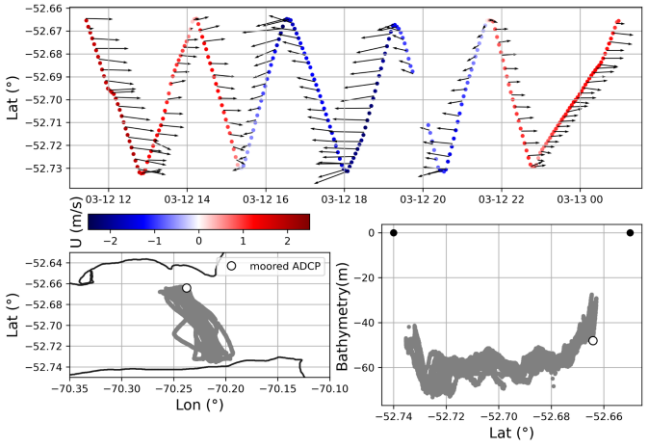

Fig. 11. Position of the cross-channel transect ADCP measurements between March 12, 2019, and March 13, 2019, in UTC time. Upper panel: Latitude position in time for the transects, the arrows represent the magnitude and direction of the depth averaged velocity. Lower left panel: geographic position of the ship ADCP transects, the white dot represents the moored ADCP position. Lower right panel: bathymetry measured during the ADCP transects for each latitude. The white dot represents the depth of the moored ADCP. The black dots represent the approximate latitude of the channel borders at the longitudes of the ADCP transects.

Fig. 12 shows a comparison between the velocity profiles collected by the vessel-mounted ADCP and the data collected by the bottom-mounted ADCP, as well as the distance between the two instruments for the 10 transects during the 13-hour survey on March 12, 2019. The vessel-mounted ADCP data indicates the velocity profiles are quite uniform mid channel (Fig. 12, top panel), with small spatial variations when the ship is far from the channel boundaries. Near the channel boundaries, where it is shallower, strong lateral shear is observed. The vessel-mounted ADCP could only measure velocity profiles down to 50 m depth, thus the bottom boundary layer was not captured mid channel, where it was deeper, up to 65 m in the area of the transects.

Velocities measured by both instruments are in agreement. However, there is a spatial phase lag in the observed velocities. For example, slack tide is observed around 15:00 hours at the bottom-mounted ADCP location, while mid channel velocity is about 1 m/s as demonstrated by the vessel-mounted ADCP data. Another example is observed around 22:30, when slack is observed mid channel and 1 m/s velocities are measured by the bottom-mounted ADCP. This phase lag will be further explored in the numerical results section.

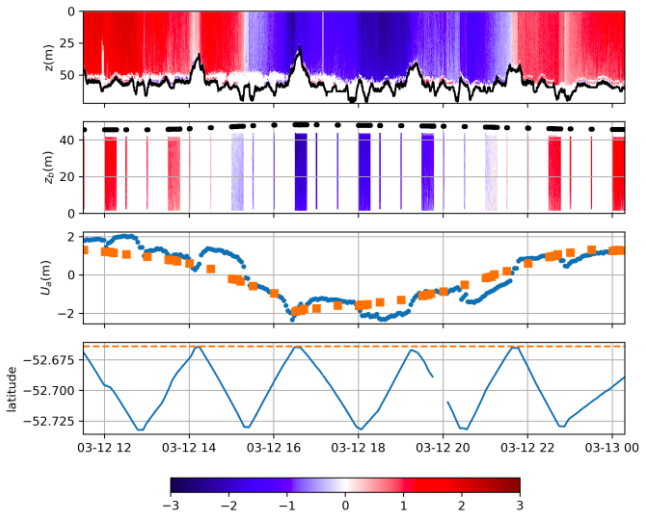

Fig. 12. Comparison of moored ADCP and ship mounted ADCP velocity profile during the ADCP transect on March 12. Upper panel: ship mounted ADCP velocity magnitude profiles; westward velocities are negative. The black line is the bottom detected from the ADCP, averaged over the 4 beams. Middle Upper panel: Moored ADCP velocity magnitude profiles. The thin rectangles represent the 90 seconds average measurements (every 30 minutes), the wide rectangles represent the 1024 seconds burst measurements. The black line represents the position of the free surface, as determined by the pressure sensor. Middle Lower panel: Depth averaged velocities Lower panel: distance between the ship mounted ADCP and the moored ADCP during the transects.

B. Numerical simulations

The model is validated in terms of tidal elevation using data from three locations: the bottom-mounted ADCP, and from two tidal gauges from IOC-UNESCO located in San Gregorio Bay (in between the two narrows) and in Punta Arenas (Fig. 13). There is a good agreement between numerical results and tidal elevation data at the three locations.

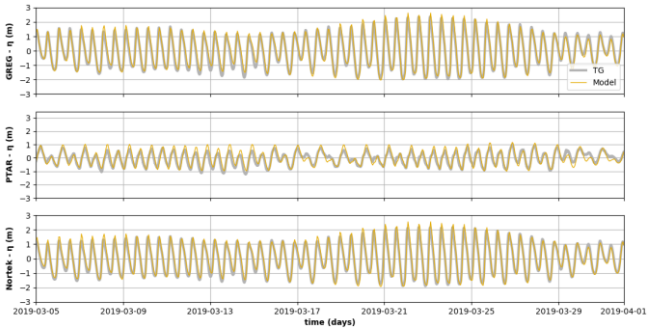

Fig. 13. Comparison between model results (in orange) and data from each tide gauge station (in grey): San Gregorio (upper panel), Punta Arenas (middle panel), and the bottom-mounted ADCP.

A comparison between the FVCOM predicted current magnitude and direction and the bottom-mounted ADCP data is presented in Fig. 14. There is also a good agreement between numerical predictions and the data. The numerical model captures the tidal modulation of the flow, although it tends to underestimate the measured velocities. The numerical model reproduces fairly well the measured flow directions and the trends observed in the data, with lower flow eastward velocities and higher westward velocities.

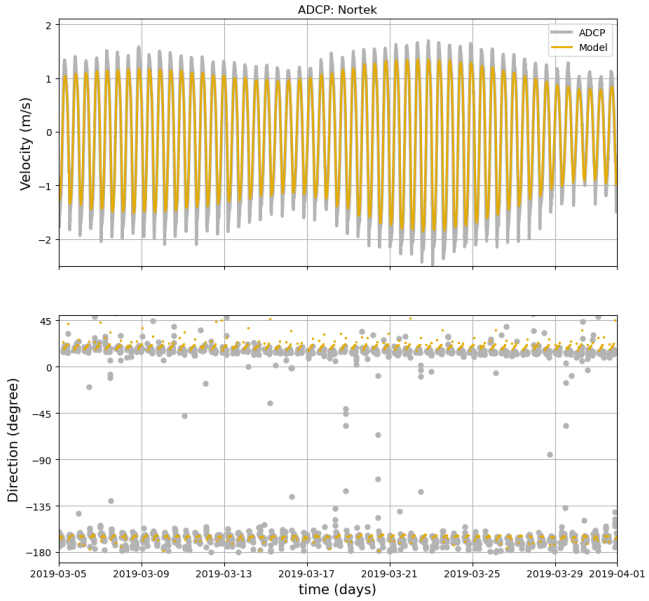

Fig. 14. Magnitude currents (upper panel) and current direction (lower panel) for the moored ADCP in gray and the numerical model in orange. The Magnitude currents are estimated using the depth-averaged velocities, the positive velocities are oriented eastward, the negative velocities are oriented westward.

The differences between the model results and the bottom-mounted ADCP data are probably explained by the large gradients observed in the bathymetry and in the velocities in the vicinity of the bottom-mounted ADCP location, which are challenging to reproduce in numerical models and require a higher accuracy in representing the bathymetry.

These differences can also be observed using harmonic analysis for the depth averaged velocity (Fig. 15). As mentioned above, the numerical model tends to underestimate the tidal harmonic amplitude for the M2, N2 and S2 harmonic components, but reproduces fairly well the tidal harmonic phases for the principal components.

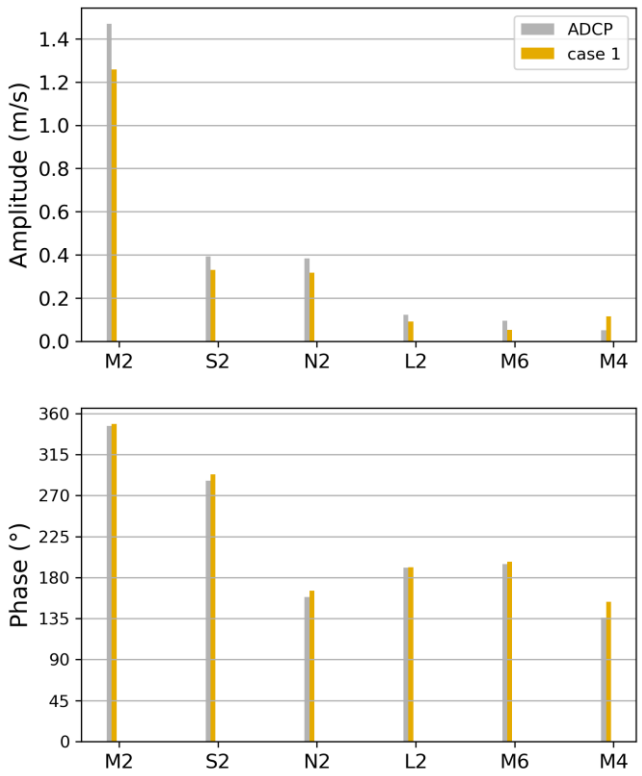

Fig 15. Comparison of the principal harmonic constituents for the depth-averaged velocity between the moored ADCP and the numerical model. Upper panel: tidal ellipse major axis amplitude. Lower panel: tidal ellipse phase.

The data obtained from the numerical model allows for comparisons with the ADCP transects velocities (Fig. 16). The observed velocity and direction spatial and temporal trends are reproduced by the model. There is a clear phase lag between the channel boundaries and the mid channel velocities, similar to what was observed in the data shown in Fig. 12. The flow is relatively uniform mid channel, with large variations in shallower waters near the channel boundaries. A sharp gradient in flow speed is observed about -52.66º latitude, where the bottom-mounted ADCP was located.

The mean depth-averaged current magnitudes obtained by the numerical model (Fig. 17.) highlight the areas of the channel suitable for tidal energy extraction. In the First Narrows, located between -69.7º and -69.3º longitude, mean velocities are higher than 1.5 m/s, during both eastward and westward flows. In the case of the Second narrows, located between -70.5º and -70.1º longitude, the mean velocities are about 1 m/s, with higher observed velocities to the west of the narrow. The mean velocities are relatively uniform across the Second narrow.

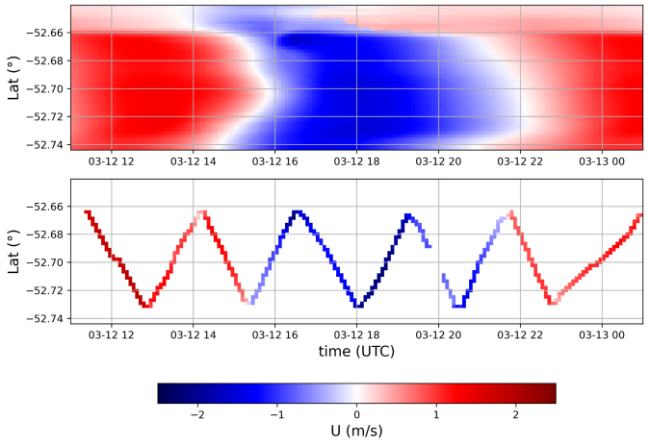

Fig. 16. Comparison of the depth-averaged velocities during the ADCP transects on March 12, 2019. The upper panel shows the depth-averaged velocity variation obtained with the numerical model in a transect at longitude -70.23 Degrees. The lower panel shows the depth-averaged velocities obtained during the ADCP transects, in a grid with the same spatial and temporal resolution of the numerical model. The moored ADCP is located at latitude -52.66 Degrees.

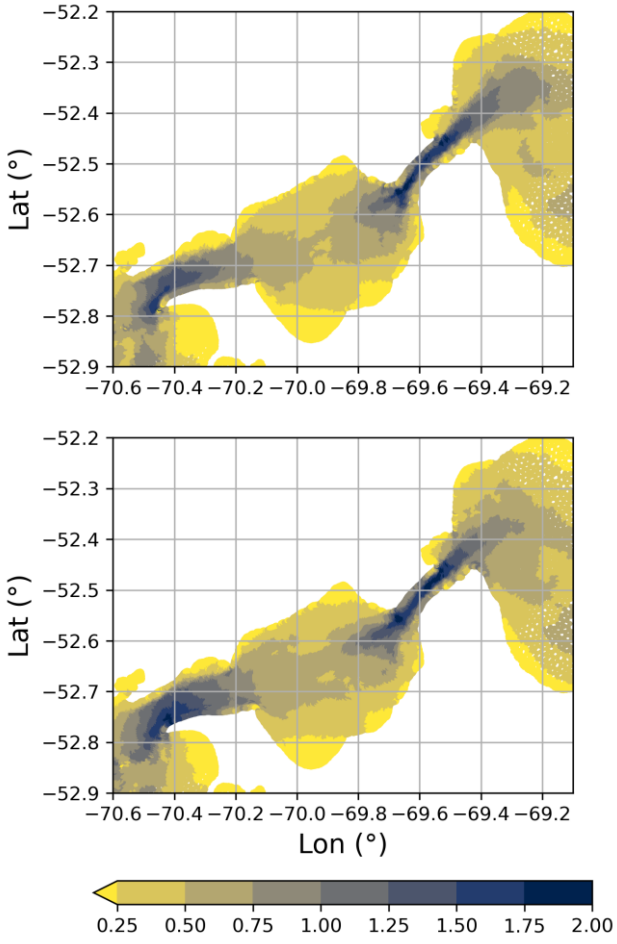

Fig 17. Mean depth-averaged current magnitude in m/s, time averaged over 40 days for eastward flows (upper panel) and westward flows (lower panel)

In terms of mean power density (Fig. 18.), the First narrows present higher power densities, up to 7 kW/m2 on average, while the Second narrow shows power densities up to 4 kW/m2. The high-power density within the two narrows is consistent for both eastward and

westward flows, meaning that the tidal energy extraction has the potential to be profitable during the whole tidal cycle.

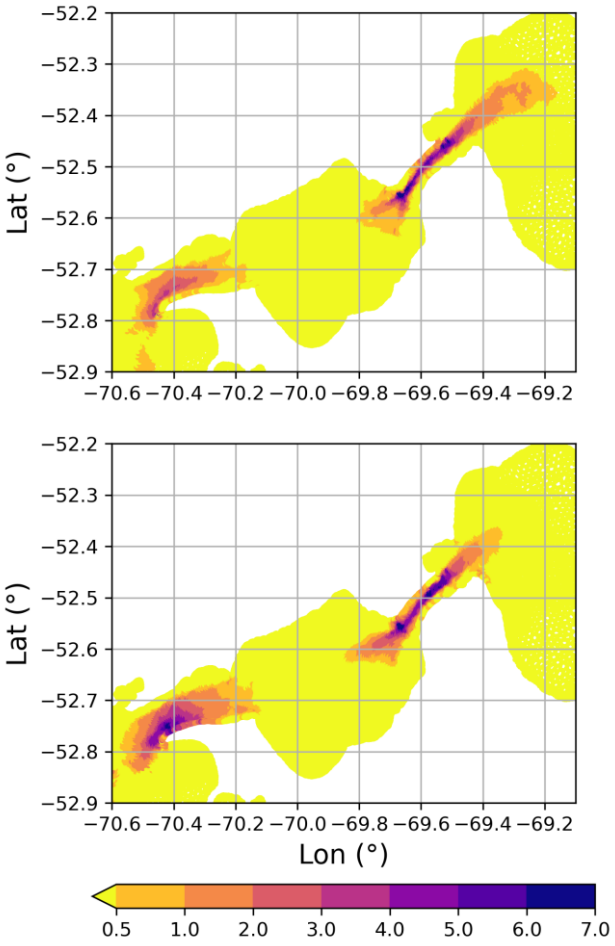

Fig. 18. Mean depth averaged power density in kW/m2, averaged over 40 days for eastward flows (upper panel) and westward flows (lower panel).

IV. Conclusion

This is the first study aimed at predicting the tidal energy resource in the Strait of Magellan, that combines both field observations and numerical simulations. Field surveys using both fixed and mobile ADCPs allow for a validation of an FVCOM numerical model of the entire Strait of Magellan. Numerical results provide a preliminary assessment at two of the Strait of Magellan main constrictions, known as the First and Second Narrows. The First narrows present higher velocities and higher power density than the Second narrows, but it is deeper (up to 80 m), and less than 4 km wide. The Second narrows also show persistent high velocities and high power density, with depths of about 60 m, and a wider cross section (7 km). Future work will focus on the interactions of physical and environmental processes that can help to promote a sustainable development of marine energies in the southern part of the continent.

Acknowledgement

This work has been supported by Chile's Marine Energy Research & Innovation Center (MERIC) CORFO project 14CEI2-28228 and VRI PUC 1566 fund. Powered@NLHPC: This research was partially supported by the supercomputing infrastructure of the NLHPC (ECM-02).

References

[1] C. Medeiros and B. Kjerfve (1988). Tidal characteristics of the Strait of Magellan. Continental Shelf Research, 8(8):947–960.}

[2] V. Combes and R.P. Matano (2018). The Patagonian shelf circulation: Drivers and variability. Progress in Oceanography 167, 24-43.

[3] M. Saraceno, E.E. D'Onofrio, M.E. Fiore, W.H. Grismeyer (2010). Tide model comparison over the Southwestern Atlantic Shelf, Continental Shelf Research 30, 1865-1875

[4] E. D. Palma and R. P. Matano (2012). A numerical study of the Magellan Plume, Journal of Geophysical Research, Vol 117, C05041.

[5] V. Combes and R. P. Matano (2014), A two-way nested simulation of the oceanic circulation in the Southwestern Atlantic, Journal of Geophysical Research Oceans, 119, 731-756.

[6] K. Guihou, A. R. Piola, E.D.Palma and M.P. Chidichimo (2020), Dynamical connections between large marine ecosystems of austral South AMerica based on numerical simulations. Ocean Sciences, 16, 271-290.

[7] M. G. Sassi and E. D. Palma (2006), Modelo Hidrodinámico del Estrecho de Magallanes, Mecánica Computacional vol XXV, pp 1461-1477.

[8] C. Chen, H. Liu and R. Beardsley (2003). An unstructured, finite-volume, three-dimensional, primitive equation ocean model: application to coastal ocean and estuaries, J. Atmos. Oceanic Technol. 20 (2003) 159–186.

[9] M. Guerra, R. Cienfuegos, J. Thomson and L. Suarez (2017). Tidal energy resource characterization in Chacao Channel, Chile, International Journal of Marine Energy 20, 1-16.

[10] T. Wang and Z. Yang (2017). A modeling study of tidal energy extraction and the associated impact on tidal circulation in a multi-inlet bay system of Puget Sound, Renewable Energy 114, 204-214.

[11] G. W. Cowles, A. R. Hakim and J. H. CHurchill, (2017). A comparison of numerical and analytical predictions of the tidal stream power resource of Massachusetts, USA, Renewable Energy 114, 215-228.

[12] Z. Yang, T. Wang, R. Branch, Z. Xiao and M. Deb (2021). Tidal stream energy resource characterization in the Salish Sea. Renewable Energy 172, 188-208.

[13] A. A. Brun, N. Ramirez, O. Pizarro, and A. R. Piola (2020). The role of the MagellanStrait on the southwest South Atlantic shelf. Estuarine, Coastal and Shelf Science, 237(February):106661

[14] GEBCO Compilation Group (2020) GEBCO 2020 Grid (doi:10.5285/a29c5465-b138-234d-e053-6c86abc040b9)

[15] G. Egbert, S. Erofeeva, Efficient inverse modeling of barotropic ocean tides, J. Atmos. Oceanic Technol. 19 (2) (2002) 183–204.

[16] P. W. Cazenave et al. (2018). PyFVCOM (version 2.2.0) [software]. Plymouth, Devon, United Kingdom: Plymouth Marine Laboratory. https://doi.org/10.5281/zenodo.1422462